Closed-form Expression for the Power Profile in Wideband Systems with Inter-channel Stimulated Raman Scattering

Lucas Alves Zischler, *Student Member, IEEE,* Chiara Lasagni, *Member, IEEE,* Paolo Serena, *Senior Member, IEEE,* Alberto Bononi, *Senior Member, IEEE,* Giammarco Di Sciullo, *Student Member, IEEE,* Divya A. Shaji, *Student Member, IEEE,* Antonio Mecozzi, *Fellow, IEEE, Optica,* and Cristian Antonelli, *Senior Member, IEEE, Fellow, Optica*

***Abstract*—Wideband systems experience significant inter-channel stimulated Raman scattering (ISRS) and channel-dependent losses. Due to the non-uniform attenuation profile, the combined effects of ISRS and fiber loss can only be accurately estimated using numerical methods. In this work, we present an approximate closed-form expression for the channels' power profile accounting for these combined effects. We validate the proposed expression against numerical solutions in the case of CLU transmission, showing high accuracy for both single-span and multi-span fiber-optic links. Additionally, we derive an inverse expression, formulated as a function of the output power, which can be utilized to target a desired optical signal-to-noise ratio (OSNR) profile through pre-emphasis of the launched channel powers.**

***Index Terms*—Non-linear effects, Wideband transmission, Wavelength-division multiplexing (WDM), Inter-channel stimulated Raman scattering (ISRS), Launch power pre-emphasis.**

I. Introduction

CAPACITY requirements have been increasing exponentially, motivating the development of novel optical systems that operate beyond traditional bands [1], [2]. *Numerous experimental studies in the literature have explored transmission over increasingly wider bandwidths. In [3], the authors investigate SCL transmission and review the multi-band technologies available at the time. In [4], [5], it is shown the transmission of ∼100 nm seamless spectra using novel semiconductor optical amplification. In [6], the authors optimize transmission capacities in a SCL setup by applying pre-emphasis to the launched power profile. In [7], throughput is improved by employing different constellations across frequency channels. In [8], the authors evaluate the benefit of utilizing distributed Raman amplification in a SCL transmission scenario.*

Manuscript received XXX xx, XXXX; revised XXXXX xx, XXXX; accepted XXXX XX, XXXX. This work was supported in part by the European Union under the Marie Skłodowska-Curie Grant Agreement No. 101120422 - Quantum Enhanced Optical Communication Network Security (QuNEST) and No. 101072409 - Optical Fiber Higher Order mode Technologies (HOMTech) (Corresponding Author: Lucas Alves Zischler)

Lucas Alves Zischler, Giammarco Di Sciullo, Divya A. Shaji, Antonio Mecozzi, and Cristian Antonelli are with the Department of Physical and Chemical Sciences, University of L'Aquila, 67100 L'Aquila, Italy: (e-mail: lucas.zischler@univaq.it).

Chiara Lasagni, Paolo Serena, and Alberto Bononi are with the Department of Engineering and Architecture, Università degli Studi di Parma, 43124 Parma, Italy.

Nevertheless, as the occupied bandwidth expands, non-linear effects and discrepancies in per-channel losses become increasingly significant [9], [10]. Although inter-channel stimulated Raman scattering (ISRS) is also a concern in conventional C-band transmission, it becomes particularly significant in wideband systems, as the Raman efficiency increases with frequency separation, reaching a peak near a 14 THz difference [11]. The combined impact of ISRS and frequency-dependent attenuation leads to noticeable distortions in the power spectral profile during propagation. This uneven power distribution can result in substantial disparities in signal-to-noise ratio (SNR) values across channels and can result in capacity penalties if not properly mitigated [12]–[15].

By shaping the launch power spectrum, it is possible to pre-compensate for frequency-dependent distortions. This is achieved through a pre-emphasis profile, the estimation of which has been the subject of many works. In [16], a closed-form expression is used to compensate for the ISRS-induced tilt in the presence of non-linear interference (NLI) for throughput maximization, but it does not address pre-compensation for channel-dependent losses. In [17], [18], iterative numerical methods are employed to minimize cost functions in order to achieve, respectively, a desired SNR profile or throughput maximization under ISRS and NLI. These approaches rely either on closed-form solutions assuming constant attenuation or on numerical solutions of the power evolution equations. *In [19], the authors employ a derivative-free optimization algorithm with closed-form Gaussian noise (GN) model expressions to optimize throughput rates in a SCL setup. The methods proposed in [19]–[24] further incorporate distributed Raman amplification and use exhaustive iterative optimization techniques for throughput optimization.*

To estimate capacity losses due to ISRS-induced distortions, pre-emphasis profiles, and NLIs, accurate estimation of how signal powers evolve along the fiber is required. In wideband systems, numerical solvers are usually employed to evaluate distortions in signal power profiles caused by ISRS and frequency-dependent attenuation, since exact closed-form solutions are known only for the special case of constant attenuation and a linear Raman gain profile, as derived by Christodoulides [25] and Zirngibl [26].

In this work, we provide an approximate closed-form solution for the signal power profiles accounting for the com-

bined effects of ISRS and frequency-dependent attenuation. Although an exact closed-form solution accounting for both ISRS and frequency-dependent attenuation is not currently available in the literature, several approximate solutions have been proposed [16], [27]–[29]. In [27], [28], a closed-form expression for the power profile evolution is derived to estimate NLI levels. That approach relies on iteratively determining power profile coefficients, initially starting from a tentative answer in order to minimize a cost function. In [29], the authors incorporate frequency-dependent attenuation into the signal power decay, while the ISRS-induced gain or loss is computed from Zirngibl's solution. The work in [16] extends Zirngibl's derivation to wider bandwidths by adopting a triangular approximation of the Raman gain profile. However, the derivation assumes a flat launch profile and constant attenuation, and the final expression replaces the constant attenuation with its frequency-dependent value.

The derivations presented in this work follow similar steps to those in Zirngibl's work, but retain the frequency dependence of the attenuation coefficient and assume a triangular approximation for the Raman gain profile, in order to derive an approximate closed-form expression for the channel power profiles. The proposed expression is based on the assumption that the total power decays exponentially along the fiber. The final solution depends on the launch power spectrum, the fiber attenuation profile, and the slope of the Raman gain profile.

The closed-form expressions are validated against numerical solutions in different multiband transmission scenarios, with a special focus on the CLU case, where we demonstrate the model's accuracy under strongly frequency-dependent fiber loss. The solution is highly accurate when the transmission bandwidth falls within close range to the Raman triangular window, such as in CLU or SCL systems, but it becomes less accurate for scenarios with increasingly wider bandwidths. We further extend the solution to a multi-span scenario, where total power loss is compensated, but no in-line per-channel power equalization is applied, and show that the model accurately estimates channel powers even in the presence of accumulated frequency-dependent loss and ISRS-induced distortion.

In addition, we provide an analytical solution to the inverse problem and demonstrate its use for pre-compensation of ISRS-induced tilt, frequency-dependent losses, and band-dependent amplified spontaneous emission (ASE) noise power. This is achieved by estimating the pre-emphasis profile that yields a desired optical signal-to-noise ratio (OSNR) output spectrum through a simple iterative approach. The solution presented in this work specifically targets a desired OSNR profile, rather than a SNR profile, as nonlinearities are not considered in our analysis*, limiting its accuracy, but significantly reducing computational complexity. The works in [17]–[24] optimize SNR profiles using broad optimization methods, where the reduction in complexity lies on employing fast and accurate GN models for NLI estimation. Even when executable in real time, such broad optimization algorithms remain computationally demanding. Simplifications can be achieved by focusing on OSNR-limited transmission scenarios. Furthermore, several studies on optimal pre-emphasis estimation for wideband transmission have shown that ASE noise is the dominant impairment [19], [20], indicating that OSNR often provides a tight upper bound to the actual SNR. Therefore, the solution presented here can be used in combination with more sophisticated methods to narrow the search space of optimization algorithms, providing a rough estimate of the optimal profile that can further be fine tuned.*

The remainder of this paper is organized as follows. In Section II, we review the fundamental equations describing ISRS in the presence of frequency-dependent loss. Section III presents the derivation of our closed-form expression for the transmitted signal powers as a function of propagation distance. In Section IV, we extend the solution to multi-span links. Section V provides modified formulas to estimate a pre-emphasis profile that achieves a desired output OSNR spectrum using the closed-form expressions. Section VI is devoted to the conclusions.

II. ISRS and Attenuation Profile Distortion on Power Spectra

The power evolution of a signal propagating at frequency f_i, in the presence of ISRS, *is known to obey* the following equation *[30, Eq. (3)] [31, Eqs. (1) and (2)]*

$$\begin{aligned}\frac{\mathrm{d}P_i(z)}{\mathrm{d}z} =& -\alpha(f_i)P_i(z) + \sum_{f_j>f_i} g_{\mathrm{R}}(f_j-f_i)P_i(z)P_j(z) \\ &- \sum_{f_j<f_i} \frac{f_i}{f_j} g_{\mathrm{R}}(f_i-f_j)P_i(z)P_j(z),\end{aligned} \tag{1}$$

where $\alpha(f)$ is the frequency-dependent attenuation coefficient, and $g_{\mathrm{R}}(\Delta f)$ is the Raman gain efficiency profile, plotted in Fig. 1, with $G_{\mathrm{R}} = \max[g_{\mathrm{R}}(\Delta f)]$ denoting the peak Raman gain efficiency. The Raman gain efficiency profile can be approximated by a triangular function with slope c_{R} and window Δ_{R}, such that $g_{\mathrm{R}}(\Delta f) \approx c_{\mathrm{R}} \cdot \Delta f \cdot H(\Delta_{\mathrm{R}} - \Delta f)$, where $H(x)$ is the Heaviside step function, as shown in Fig. 1. *Within operational regimes of optical transmission, the contribution of NLI to the total signal power is negligible. Therefore, although NLI contribute to signal degradation, the accuracy of* (1) *is not reduced by its neglect.*

The intensity of stimulated Raman scattering between two fields at two different frequencies is proportional to the overlap integral of the fields' lateral profiles, which is equal to the inverse of the effective mode area [32, Eq. (33)], making the Raman gain coefficient a bivariate function. This dependence is influenced by the fiber design [33], and therefore the actual Raman gain response is highly specific to a given scenario. Nevertheless, experimental validations of closed-form SNR expressions that neglect this frequency dependence have shown high accuracy in the SCL transmission window with E-band Raman pumps [23], [34], supporting the use of a frequency-independent approximation for the Raman gain slope. However, this dependence remains crucial in ultrawideband scenarios, where effective area values may diverge significantly across the transmission window [24].

Losses in standard single-mode fibers (SSMFs) typically exhibit a parabolic profile, with a global minimum located

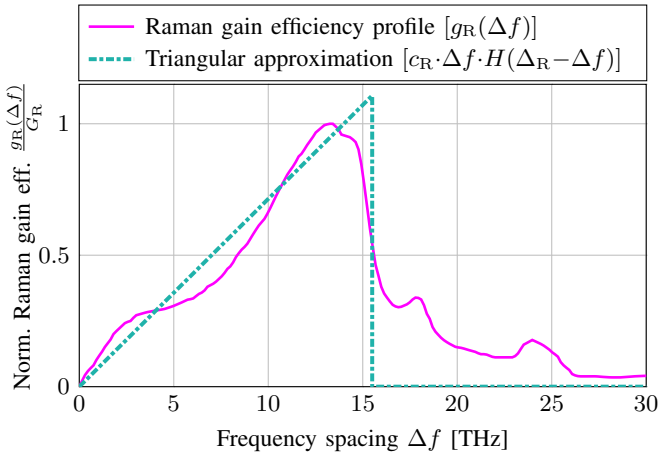

Fig. 1: Normalized Raman gain efficiency profile based on [35], [36], shown alongside its first-order and triangular approximations. The triangular model assumes the actual peak at $\Delta f = 14$ THz ($c_R = G_R/14$ THz) and spans a window of $\Delta_R = 15.5$ THz. In the legend, $H(x)$ represents the Heaviside step function.

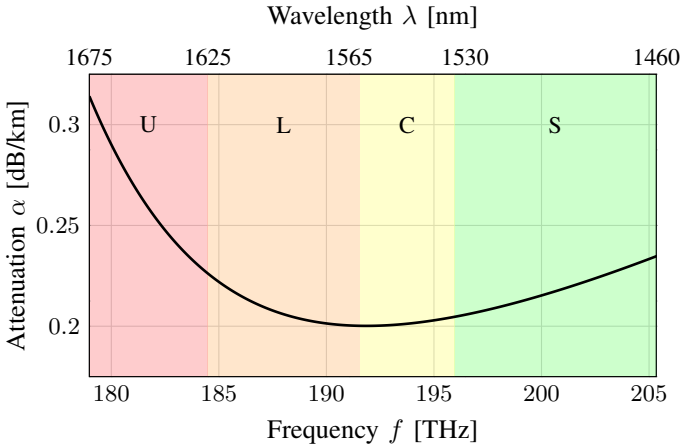

Fig. 2: Attenuation profile for a doped silica fiber [37] and bands of transmission [2].

within the C-band. The attenuation profile assumed in this work is shown in Fig. 2.

Frequency-dependent losses are linear effects and can, in principle, be compensated in regions where non-linearities are negligible, since each channel can be treated independently. Nevertheless, the presence of ISRS adds significant complexity into any compensation technique, as the power levels of different channels become correlated with each other due to Eq. (1). Within conventional bands, assuming a constant attenuation profile, a closed-form solution for the ISRS-induced tilt was derived in [25], [26]. However, as seen in Fig. 2, this assumption becomes increasingly inaccurate as the bandwidth extends beyond the C-band, making the interplay between ISRS and attenuation difficult to evaluate.

Disregarding frequency conversion losses ($f_i/f_j \approx 1$), and assuming infinitely many equally spaced channels between f_{Min} and f_{Max} such that the per-channel power converges to the power spectral density, Eq. (1) becomes

$$\frac{\partial S(f,z)}{\partial z} = -\alpha(f)S(f,z) + c_{\mathrm{R}} S(f,z)\int_{f-\Delta_{\mathrm{R}}}^{f+\Delta_{\mathrm{R}}} (f'-f)S(f',z)\mathrm{d}f', \tag{2}$$

where $S(f,z)$ is non-zero only within the allocated spectrum, i.e., $S(f,z) = 0$ for $f \notin (f_{\mathrm{Min}}, f_{\mathrm{Max}})$. No exact closed-form solution is known for $S(f,z)$ for frequency-dependent $\alpha(f)$.

III. Closed-Form Expressions for the Power Profiles

The main result of this work is the following expression for the spectral density profile, whose derivation is presented in Appendix A

$$S(f,z) = S(f,0)\exp\left[-\alpha(f)z + c_{\mathrm{R}}(\Gamma(f_{\mathrm{R}}) - \Gamma(f))\int_0^z P_{\mathrm{T}}(z')\mathrm{d}z'\right], \tag{3}$$

where $P_{\mathrm{T}}(z)$ is the total power at position z, $\Gamma(f)$ is a shaping function accounting for the powers involved in the ISRS process, and f_{R} is a reference frequency with no ISRS-induced tilt. The shaping function is given by

$$\Gamma(f) = \int_{f_{\mathrm{Min}}}^{f} \frac{P_\Delta(f',0) - \Delta_{\mathrm{R}}\left[S(f'+\Delta_{\mathrm{R}},0) - S(f-\Delta_{\mathrm{R}},0)\right]}{P_{\mathrm{T}}(0)}\mathrm{d}f', \tag{4}$$

where $P_\Delta(f,z)$ represents the total power within the $\pm\Delta_{\mathrm{R}}$ Raman triangular window

$$P_\Delta(f,z) = \int_{f-\Delta_{\mathrm{R}}}^{f+\Delta_{\mathrm{R}}} S(f,z)df. \tag{5}$$

In (4), $\Gamma(f)$ is proportional to [16, Eq. (18)] for a flat launch profile. For bandwidths smaller than Δ_{R}, $\Gamma(f)$ simplifies to

$$\Gamma(f) = f - f_{\mathrm{Min}}, \ (f_{\mathrm{Max}} - f_{\mathrm{Min}}) < \Delta_{\mathrm{R}}. \tag{6}$$

In our derivation leading to (3), the powers involved in the ISRS process at frequency f are assumed to decay proportionally to the total power. However, this assumption becomes increasingly inaccurate as the bandwidth increases, since the powers within the ISRS window account for an increasingly smaller fraction of the total power.

Integrating (2) over the entire spectrum nullifies the ISRS contribution

$$\int_{f_{\mathrm{Min}}}^{f_{\mathrm{Max}}} \frac{\partial S(f,z)}{\partial z}\mathrm{d}f = \frac{\mathrm{d}P_{\mathrm{T}}(z)}{\mathrm{d}z} = -\int_{f_{\mathrm{Min}}}^{f_{\mathrm{Max}}} \alpha(f)S(f,z)\mathrm{d}f, \tag{7}$$

where $P_{\mathrm{T}}(z)$ is the total power within the entire occupied spectrum. Therefore, the instantaneous total power evolution is dictated solely by the attenuation and the power spectral profile, suggesting a weak contribution of ISRS in the total power decay. Under constant attenuation, the total power evolution is dictated only by the constant attenuation coefficient, as shown in [26]. However, since ISRS shapes the power spectral distribution, it has an indirect effect on the total power longitudinal profile. Nevertheless, we assume an exponential decay of the total power, governed by a single

effective attenuation coefficient α_0, i.e., $P_{\mathrm{T}}(z) \approx P_{\mathrm{T}}(0)e^{-\alpha_0 z}$. The total power integral in (3) can then be approximated by

$$\int_0^z P_{\mathrm{T}}(z')\mathrm{d}z' \approx P_{\mathrm{T}}(0)\frac{1-e^{-\alpha_0 z}}{\alpha_0}. \tag{8}$$

The total power attenuation coefficient can be obtained from (Derived in Appendix B)

$$\alpha_0 \approx \sqrt[n]{\int_{f_{\mathrm{Min}}}^{f_{\mathrm{Max}}} \frac{\alpha^n(f')S(f',0)}{P_{\mathrm{T}}(0)}\mathrm{d}f'}, \tag{9}$$

where $n \in \mathbb{N}^+$ is a free parameter, arising as a byproduct of the exponential approximation for the total power decay, as shown in Appendix B (see Eqs. (33) and (34)). The parameter n provides an additional degree of freedom when applying the model, and can be universally optimized, as is discussed further in Sec. III-A.

From the assumption of an exponential total power decay, we can also derive an expression for the shaping function at the zero-ISRS-induced-tilt frequency[1] $\Gamma(f_{\mathrm{R}})$ as (Derived in Appendix C)

$$\Gamma(f_{\mathrm{R}}) \approx \frac{-1}{c_{\mathrm{R}}P_{\mathrm{T}}(0)L_{\mathrm{eff}}} \ln\left[\int_{f_{\mathrm{Min}}}^{f_{\mathrm{Max}}} \frac{\alpha^n(f')S(f',0)}{\alpha_0^n P_{\mathrm{T}}(0)} \times e^{[\alpha_0-\alpha(f')]L - c_{\mathrm{R}}\Gamma(f')P_{\mathrm{T}}(0)L_{\mathrm{eff}}}\mathrm{d}f'\right], \tag{10}$$

where $L_{\mathrm{eff}} = (1-e^{-\alpha_0 L})/\alpha_0$ is the effective length of the total power profile, with L denoting the fiber length. Replacing (8) in (3) yields

$$S(f,z) = S(f,0)e^{-\alpha(f)z + c_{\mathrm{R}}(\Gamma(f_{\mathrm{R}})-\Gamma(f))P_{\mathrm{T}}(0)\left(1-e^{-\alpha_0 z}\right)/\alpha_0}. \tag{11}$$

Representing the signal as a finite sequence of CW tones, we arrive at a closed-form expression for the power profile of the propagated signals[2]

$$P_i(z) = P_i(0)e^{-\alpha_i z + c_{\mathrm{R}}(\Gamma(f_{\mathrm{R}})-\Gamma(f_i))P_{\mathrm{T}}(0)\left(1-e^{-\alpha_0 z}\right)/\alpha_0}. \tag{12}$$

With finitely many discrete channels, the integrals in (9) and (10) are replaced by summations over the allocated channels, resulting in a complete closed-form solution. The shaping function $\Gamma(f)$ becomes

$$\Gamma(f_i) = \frac{\sum_{j=0}^{i} B_s \sum_{|f_k - f_i| < \Delta_{\mathrm{R}}} P_k(0) - \Delta_{\mathrm{R}}\left[P_{j+\left\lfloor\frac{\Delta_{\mathrm{R}}}{B_s}\right\rfloor}(0) + P_{j-\left\lfloor\frac{\Delta_{\mathrm{R}}}{B_s}\right\rfloor}(0)\right]}{P_{\mathrm{T}}(0)}, \tag{13}$$

where B_s is the frequency channel spacing.

[1]The value of $\Gamma(f_{\mathrm{R}})$ ensures energy conservation in ISRS and is, strictly speaking, z-dependent. However, for simplicity, we evaluate it only at $z = L$ where the power profile is most relevant, and assume it to be constant over the fiber length. A more accurate power evolution profile over the entire span can be obtained by evaluating (10) on the entirety of the z domain, rather than just at $z = L$.

[2]*A implementation of the closed-form equations shown in this work is available online at https://gitlab.com/lucaszischler/closed-form-isrs-wideband.*

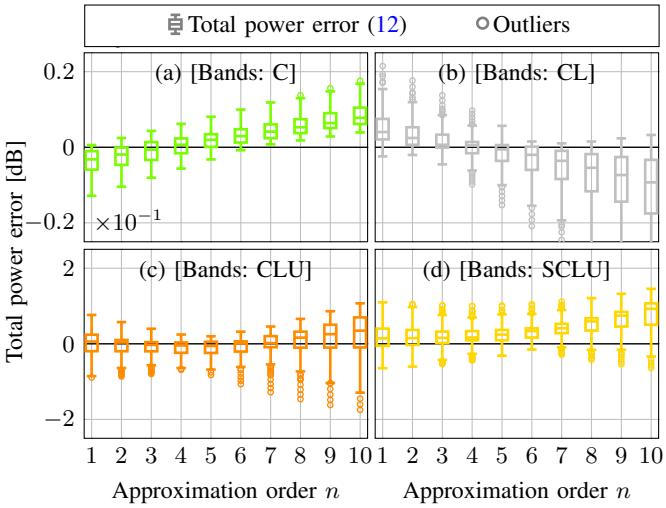

Fig. 3: Box plots of the total power error ratio ϵ_P of the closed-form approximation, defined in (14), as a function of the approximation order n. Each data point corresponds to a unique combination of G_{R}, $P_i(0)$, and L. The multiplicative factor shown in the lower-right corner of (a) indicates the scaling factor of the y-axis. Markers represent outlier values beyond 1.5 times the interquartile range.

A. Numerical validation

We start by evaluating the impact of the approximation order n on the accuracy of the closed-form solution. To quantify the accuracy of the approximation, we define the total power error ratio at the fiber output as

$$\epsilon_P = \frac{\sum_{i=1}^{N_{\mathrm{ch}}} P_i(L)}{\sum_{i=1}^{N_{\mathrm{ch}}} \widehat{P}_i(L)}, \tag{14}$$

where N_{ch} is the channel count, $\widehat{P}_i(z)$ are the numerically computed power profiles from (1), and $P_i(z)$ are the closed-form results from (12). We evaluate n over practical values for the Raman gain peak efficiency G_{R}, per-channel launch power $P_i(0)$, and fiber length L, across four bandwidth scenarios (C-band, CL, CLU, and SCLU). Channel spacing is assumed to be 50 GHz. Each variable is swept over 5 evenly spaced values within the following domains: $G_{\mathrm{R}} \in (0.3, 0.4)$ 1/W/km, $P_i(0) \in (-5, 0)$ dBm, and $L \in (50, 150)$ km, for a total of 125 configurations for each bandwidth. The Raman gain slope coefficient c_{R} considers the actual peak at 14 THz and triangular approximation with bandwidth Δ_{R} of 15.5 THz. The actual Raman gain efficiency profile and triangular approximation shown in Fig. 1, based on data from [36]. The considered attenuation profile shown in Fig. 2, derived from [37]. The power evolution equations are solved numerically using a 4^{th} order Runge-Kutta method over 50 equal-length segments along the fiber span, with initial conditions defined by the channels launch powers.

The results are shown in Fig. 3, where each subplot refers to a specific bandwidth scenario. We see in Fig. 3(a) negligible error values for a C-band only scenario, regardless of the choice of n. In Figs. 3(b–d), approximation orders $n = 3$

Spans	Parameter	Value
	Raman gain peak G_{R}	0.4/W/km
	Raman gain eff. profile first-order coefficient c_{R} (14 THz)	0.0286/W/km/THz
	Channel spacing B_s	50 GHz
	Per-channel launch power $P_i(0)$	-1 dBm
	Approximation order coefficient n	3
Single	Length L	100 km
Multi	Span length L_s	50 km
	Total length L	250 km
	Simulation sections per span	50

Bands	C	CL	CLU	SCL	SCLU
Bandwidth [THz]	4.05	11.15	16.65	20.90	26.05
Channel count	81	223	333	418	521

TABLE I: Simulation parameters. Some parameters are specific to either single-span or multi-span scenarios.

or $n = 4$ produce the lowest average errors over all evaluated bandwidth sizes.

All subsequent simulations use the parameter values listed in Table I, with Raman gain efficiency and attenuation profiles shown in Fig. 1 and Fig. 2, respectively.

Figure 4 compares the derived closed-form expressions with numerical solutions from (1) as a function of propagation distance for a CLU transmission scenario, *where the fiber loss coefficient is strongly frequency-dependent*. The total power longitudinal profile follows the exponential assumption closely. Colored lines correspond to channels at the edges of the transmitted bands, with the closed-form solution given by (12). The inset of Fig. 4 compares the analytical and numerical power profiles at the fiber output. The excellent agreement between the two is self-evident.

In Fig. 5, the closed-form solution is evaluated for increasingly wider bandwidths, using the parameter values listed in Table I for a single-span scenario. Figures 5(a) and 5(b) indicate that the closed-form solutions are in excellent agreement with the numerical results when the considered spectrum does not greatly exceed the Raman triangular window. In Figs. 5(c–d), the closed-form results underestimate the magnitude of the ISRS-induced tilt. This discrepancy is possibly due to our approximation that the total power within the Raman triangular window is exponentially decaying, with equal rate as the total bandwidth power.

IV. Closed-form Expressions for Uncompensated Multi-Span Systems

The closed-form expression given in (12) describes the signal evolution along an unrepeated link. The ISRS-induced tilt predominantly accumulates near the fiber input, where the total power $P_{\mathrm{T}}(z)$ is highest. As the total power attenuates along the fiber, the ISRS-induced tilt increment vanishes. However, when signals are reamplified, the ISRS-induced tilt increases again. With the combined effects of ISRS and frequency-dependent losses, the power spectral profile can accumulate significant distortion over multiple uncompensated spans.

In-line amplifiers typically provide a constant gain over their operating bandwidth, with the gain value often being the sole adjustable parameter. An uneven gain profile can be equalized within the same amplification device with the

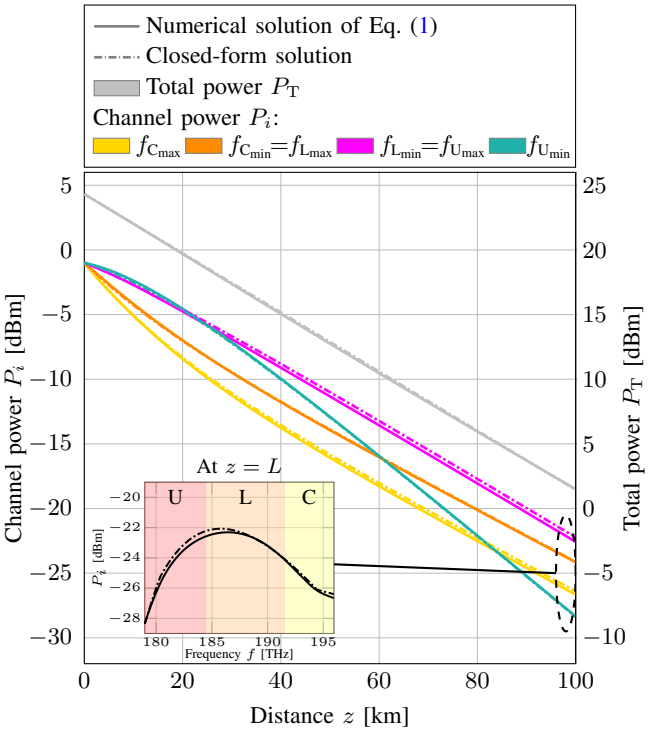

Fig. 4: Longitudinal profiles of the total power and selected channels at the edges of the transmitted bands for a single-span CLU transmission, using the parameters in Table I. Numerical solutions are shown as solid lines, while closed-form expressions are shown as dash-dotted lines. The closed-form solution is given by (12) for individual channel powers and by $P_{\mathrm{T}}(z) = P_{\mathrm{T}}(0)e^{-\alpha_0 z}$ for the total power. The inset shows the power spectral profile at the fiber output ($z = L$).

aid of Gain flattening filters (GFFs). However, unless explicit information of the fiber link is provided to the amplifier, GFFs do not compensate for channel-dependent losses. To mitigate accumulated distortions, long-haul links often employ dynamic gain equalizers (DGEs) *typically* every 5^{th} span to restore power levels [13], [38], [39]. Even if desired, incorporating DGEs in each in-line amplification device incurs in additional cost to the setup, so accumulated levels of ISRS-induced distortion are expected in practical links.

In multi-band scenarios, different amplifiers are employed to cover distinct portions of the spectrum [40]. These amplifiers maintain total power levels within their respective windows, providing some degree of distortion compensation. Nevertheless, in-band distortions can still accumulate in a multi-span link.

Using (12), we can also derive expressions for the signal profiles accounting for accumulated ISRS-induced tilt and frequency-dependent losses over multiple spans. We consider a worst-case scenario where the amplification gain is uniform across the entire spectrum, even in a multi-band system, and is determined solely by the total power. Under this scenario, the total power at the beginning of any k^{th} span remains constant ($P_{\mathrm{T}}^{(k)}(0) = P_{\mathrm{T}}^{(1)}(0)$), and the gain of the $(k+1)^{\mathrm{th}}$ in-line

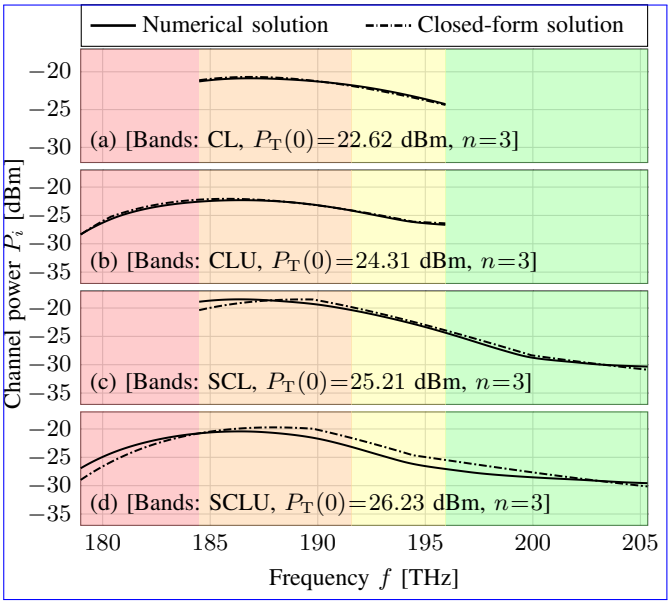

Fig. 5: Power spectral profiles for increasingly wider bandwidths using the parameters in Table I. Numerical solutions are shown as solid lines, while closed-form expressions are shown as dash-dotted lines. The corresponding total launch powers $P_{\mathrm{T}}(0)$ and approximation order coefficient n used are displayed in the figure.

amplifier is equal to the total loss of the previous span

$$G^{(k+1)} = \int_{f_{\mathrm{Min}}}^{f_{\mathrm{Max}}} \frac{S^{(k)}(f', L)}{P_{\mathrm{T}}^{(1)}(0)} \mathrm{d}f', \tag{15}$$

where the output power spectral profile of each span can then be obtained from (11) with the respective span parameters. *The gain value in (15) is assumed to be constant over the evaluated spectrum. For a multi-band amplification scenario with constant per-band total power, the gain varies over frequency and can be trivially accounted for in our equations by replacing $G^{(k)}$ with its frequency-dependent value. Other schemes can be incorporated if the gain function is known. The gain is assumed to be lumped at the beginning of each span.*

Assuming homogeneous spans, the power spectral density at the beginning of the $(k+1)^{\mathrm{th}}$ span is given iteratively from the powers of the previous span by

$$S^{(k+1)}(f,0) = S^{(k)}(f,0) G^{(k+1)} \times e^{-\alpha(f)L_s + c_{\mathrm{R}}[\Gamma^{(k)}(f_{\mathrm{R}}^{(k)}) - \Gamma^{(k)}(f)] P_{\mathrm{T}}(0) L_{\mathrm{eff}}^{(k)}}, \tag{16}$$

where the effective length $L_{\mathrm{eff}}^{(k)}$ and the shaping function $\Gamma^{(k)}(f)$ depend on the input spectral profile and the total power attenuation coefficient for the k^{th} span. Given the launch power spectral density of the first span $S^{(1)}(f,0)$, we can iteratively compute the per-span values of $\alpha_0^{(k)}$, $\Gamma^{(k)}(f)$, $\Gamma^{(k)}(f_{\mathrm{R}}^{(k)})$, $G^{(k)}$, and $S^{(k)}(f,0)$ using (9), (4), (10), (15), and (16), respectively. The power profile at any distance along the link can then be obtained from (11) with the corresponding span parameters.

In Fig. 6(a) and 6(b), we compare numerical and analytical solutions for the longitudinal and spectral power profiles respectively, using the parameter values listed in Table I for a CLU transmission setting. The numerical solution is obtained from (1), solved via the Runge-Kutta 4$^{\mathrm{th}}$ order method. At the end of each span ($z = k \cdot L_s$), the power profiles are normalized so that the total power equals the initial launch power, thereby emulating the assumed amplification. The results show excellent agreement between numerical and analytical curves.

V. Pre-Emphasis Estimation

The formulas provided so far require the values of the initial power profile in order to estimate the total attenuation coefficient α_0, the shaping profile $\Gamma(f)$, and the shaping function at the zero-ISRS-induced-tilt frequency $\Gamma(f_{\mathrm{R}})$. However, for pre-emphasis estimation, the output power spectral profile is set, and the input spectrum is to be determined. In what follows we derive the relevant expressions that are necessary to solve this problem.

As the shaping profile $\Gamma(f)$ is assumed to be z-independent, as discussed in Appendix A, it can be estimated from the output profile with

$$\Gamma(f) = \int_{f_{\mathrm{Min}}}^{f} \frac{P_{\Delta}(f';L) - \Delta_{\mathrm{R}} \left[S(f'+\Delta_{\mathrm{R}}, L) - S(f-\Delta_{\mathrm{R}}, L)\right]}{P_{\mathrm{T}}(L)} \mathrm{d}f'. \tag{17}$$

Following the previously discussed approximations, we can also obtain α_0 and $\Gamma(f_{\mathrm{R}})$ as functions of the output powers, as given respectively by (Derived in Appendix D)

$$\alpha_0 \approx \sqrt[n]{\int_{f_{\mathrm{Min}}}^{f_{\mathrm{Max}}} \frac{\alpha^n(f') S(f', L)}{P_{\mathrm{T}}(L)} \mathrm{d}f'}, \tag{18}$$

$$\Gamma(f_{\mathrm{R}}) \approx \int_{f_{\mathrm{Min}}}^{f_{\mathrm{Max}}} \frac{\Gamma(f') \alpha^n(f') S(f', L)}{\alpha_0^n P_{\mathrm{T}}(L)} \mathrm{d}f'. \tag{19}$$

With (18) and (19), we can obtain the input spectral profile that results in any arbitrary power profile at the fiber output

$$S(f,0) = S(f,L) e^{\alpha(f)L - c_{\mathrm{R}}(\Gamma(f_{\mathrm{R}}) - \Gamma(f)) P_{\mathrm{T}}(L) \left(e^{\alpha_0 L} - 1\right)/\alpha_0}. \tag{20}$$

In some scenarios, setting the absolute values of the received powers for individual channels is not required, and only their relative powers are relevant. In such cases, we can replace the power spectral density profile in (18) and (19) with a normalized profile, where only its shape is relevant, namely

$$\begin{aligned} \widetilde{S}(f,L) &= \frac{S(f,L)}{P_{\mathrm{T}}(L)}, \\ \widetilde{P}_{\Delta}(f,L) &= \frac{P_{\Delta}(f,L)}{P_{\mathrm{T}}(L)}. \end{aligned} \tag{21}$$

With an added constraint on the total input power, we can obtain the actual output profile values. From the integration of (20) over the entire band, by rewriting the total power integral as a function of the total input power as given by (8),

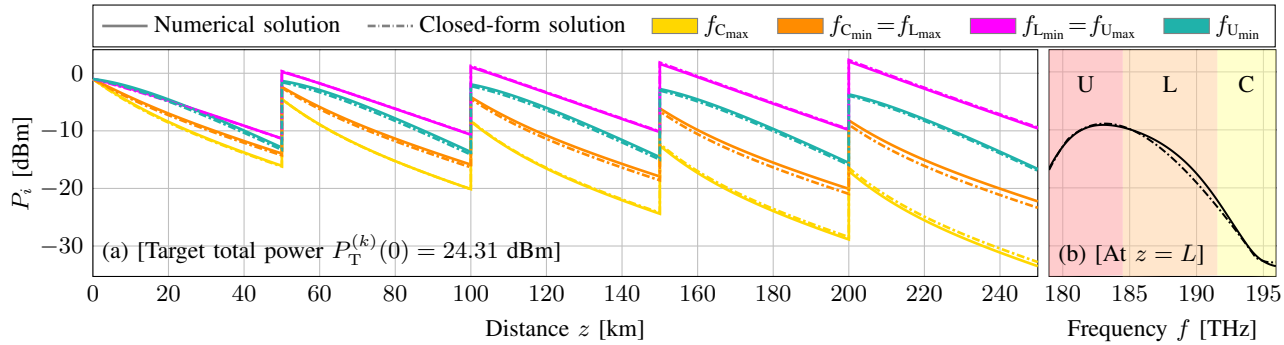

Fig. 6: (a) Power profiles of selected channels at the edges of the transmitted bands, obtained via numerical methods, shown in solid lines, and closed-form expressions, shown in dash-dotted lines, considering the parameters listed in Table I for a multi-span link and CLU transmission. (b) Power spectral profile at the link end ($z = L$).

and after some manipulation, the total output power can be obtained in the following form

$$P_{\mathrm{T}}(L) = \int_{f_{\mathrm{Min}}}^{f_{\mathrm{Max}}} \frac{P_{\mathrm{T}}(0)}{\widetilde{S}(f', L)} e^{-\alpha(f')L + c_{\mathrm{R}}(\Gamma(f_{\mathrm{R}}) - \Gamma(f'))P_{\mathrm{T}}(0)L_{\mathrm{eff}}} \mathrm{d}f'. \tag{22}$$

Multi-span pre-emphasis estimation can be performed with a similar approach to that of Section IV, where, for each span, we obtain a total power attenuation coefficient, reference frequency, and input power spectral profile. Under the constant total output power amplification scheme, the total per-span input power is an added constraint. In such cases, we can only estimate the pre-emphasis for a given normalized output power profile, as given in (21). The $(k-1)^{\mathrm{th}}$-span output power spectral profile is then iteratively obtained by

$$S^{(k-1)}(f,L) = \frac{S^{(k)}(f,L)}{G^{(k)}} e^{\alpha(f)L_s - c_{\mathrm{R}}(\Gamma^{(k)}(f_{\mathrm{R}}^{(k)}) - \Gamma^{(k)}(f))P_{\mathrm{T}}(0)L_{\mathrm{eff}}^{(k)}}. \tag{23}$$

The input power spectrum of any span can be obtained from (20), using the solutions from (23) and the respective span parameters.

A. OSNR profile estimation

The solutions in (20) and (23) provide the power profiles. Nevertheless, it is often desirable to attain a given OSNR profile. Disregarding non-linear effects, the closed-form solutions provided allow us to estimate a pre-emphasis profile for a desired OSNR profile using a simple iterative approach.

With (23) and (15), we are able to obtain the signal power profiles and per-span gains, respectively. *In relevant transmission settings, the intensity of the amplification noise is negligible compared to the propagating signal, with insignificant impact on ISRS. Therefore, we assume that its power evolves proportionally to the signal power, as given by*

$$S_{\mathrm{ASE}}^{(k)}(f,z) = S_{\mathrm{ASE}}^{(k)}(f,0) \frac{S^{(k)}(f,z)}{S^{(k)}(f,0)}, \tag{24}$$

where $S_{\mathrm{ASE}}^{(k)}(f,z)$ is the accumulated ASE noise power at the k^{th} span. With the per-span gain values $G^{(k)}$, amplification noise figures, and the evolution profiles from (24), we are able to obtain the optical noise profiles at the link end ($z = L$). We assume that the noise powers are sufficiently low with respect to signal power values, such that they have no influence on the ISRS-induced tilt.

As the total power constrain is at the beginning of each span in a multi-span scenario, due to in-line amplification, the actual output power values cannot be targeted. Nevertheless, normalized power values and OSNR can be targeted, where the actual values are derived from the constrain condition. Given a desired normalized OSNR profile $\widetilde{\mathrm{OSNR}}$, we can first assume that the normalized received powers $\widetilde{S}(f,L)$ have the same shape ($\widetilde{S}(f,L) \leftarrow \widetilde{\mathrm{OSNR}}$), and obtain an estimated normalized $\widehat{\mathrm{OSNR}}$ using the noise profiles from (24). We then update the received power profile with

$$\widetilde{S}(f,L) \leftarrow \widetilde{S}(f,L) \left(\frac{\widetilde{\mathrm{OSNR}}}{\widehat{\mathrm{OSNR}}} \right)^{\xi}, \tag{25}$$

where ξ is a step factor.

Figure 7 shows the profiles for an estimated launch power pre-emphasis that targets a flat OSNR over the CLU band. *In the figure, solid and dash-dotted lines represent numerical solutions of (1) using, respectively, the estimated optimal pre-emphasis profile and a flat profile with equal total power. The dotted curves correspond to the closed-form solutions.* Except for the per-channel launch powers, the simulation parameters are given in Table I for a multi-span scenario. The amplifier noise figures are 5.5 dB for the C-band, 6.0 dB for the L-band, and 5.0 dB for the U-band [40], [41]. We disregard additive noise at the transmitter and assume a boosting stage at the receiver such that the total received power equals the total launch power. We iterate the normalized received profile using (25) with a step coefficient of $\xi = 1$, until the root-mean-squared error (RMSE) between the desired and estimated normalized OSNR over all frequency channels is smaller than 10^{-5}. We achieve this RMSE value within 8 iterations.

Figure 7(a) shows that the estimated pre-emphasis results in slight offsets within the bands due to the different noise figure values. In Fig. 7(b) and (c), we see the received signal and noise powers, respectively. Without pre-emphasis, the received noise profile is overall smaller, but signal powers within the C-band are significantly lower due to ISRS power transfer

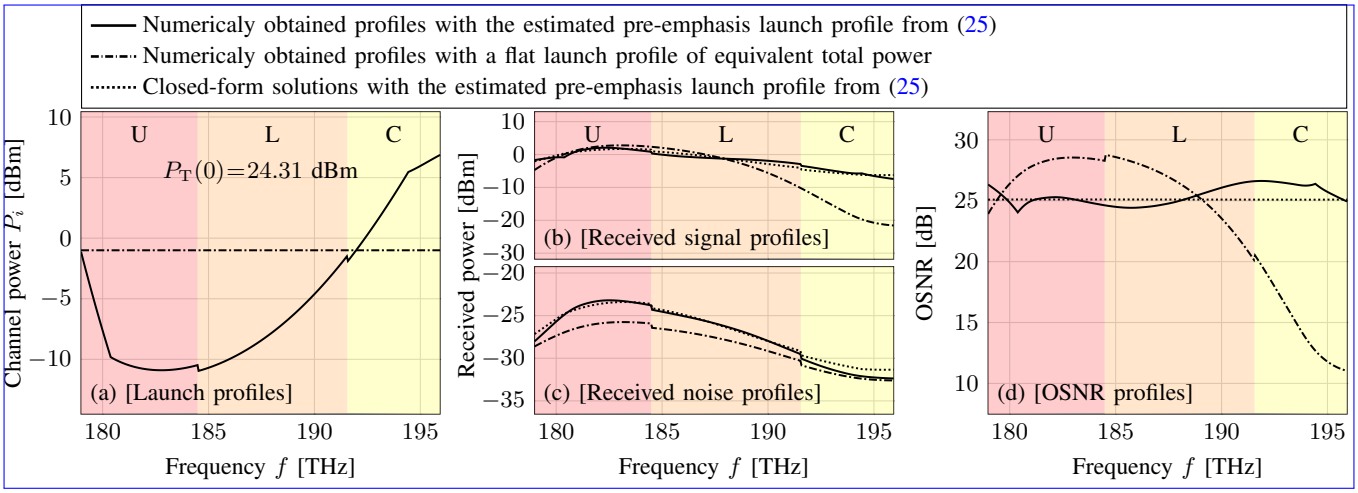

Fig. 7: (a) Launch power profiles with equal total launch power. (b, c) Received signal and accumulated ASE noise profiles, respectively, after the boosting stage at the receiver. (d) OSNR profiles for the considered launch profiles. In solid lines we have the *numerically obtained* profiles considering the estimated pre-emphasis targeting a flat OSNR *from* (25). In dash-dotted lines we show, for comparison, the *numerically obtained* profiles considering a flat launch profile with equal power as the estimated pre-emphasis. The profiles derived from the closed-form solutions are presented alongside the numerical results in (b, c, d) with dotted lines.

to the lower bands. The pre-emphasis profile compensates for this with higher launch powers within the C-band and reduced launch powers within the LU bands. In Fig. 7(d), we observe the resulting OSNR profiles. With the pre-emphasis profile, we obtain a peak-to-peak OSNR deviation of 2.58 dB, compared to a deviation of 17.73 dB with a flat launch profile.

VI. Conclusion

In this paper, we derived a closed-form expression for the signal power profiles under the effects of ISRS and frequency-dependent attenuation. As both ISRS and per-channel losses alter the power profile during propagation, the solution is non-trivial and relies on certain approximations. We assume that the effect of ISRS on the total power is negligible and that the total power decays exponentially. The approximated closed-form expressions for both total and per-channel powers show strong agreement with numerical solutions.

From the single-span solution, we extend the expression for an uncompensated multi-span scenario, where distortions due to ISRS and frequency-dependent attenuation accumulate at each span. The closed-form expression continues to show excellent agreement with numerical simulations.

We also present modified expressions for the approximated coefficients, reformulated as functions of the output powers. These expressions are then used to achieve a desired OSNR profile at the receiver through an iterative approach. We validate the expressions in a CLU-band scenario for a multi-span link. The resulting output profiles demonstrate significant improvement in the shape of the received signal.

Appendix A
Derivation of Power Spectral Profile Given ISRS and Frequency-Dependent Attenuation

In this section, we follow similar steps to those derived by Zirngibl [26] and Lasagni [16], with modifications to account for the frequency dependence of the attenuation coefficient throughout the derivation process. Dividing both sides of (2) by $S(f,z)$ and differentiating with respect to f

$$\frac{\partial}{\partial f}\left[\frac{1}{S(f,z)}\frac{\partial S(f,z)}{\partial z}\right]=-\frac{\mathrm{d}\alpha(f)}{\mathrm{d}f}+c_{\mathrm{R}}\frac{\partial}{\partial f}\int_{f-\Delta_{\mathrm{R}}}^{f+\Delta_{\mathrm{R}}}(f'-f)S(f',z)\mathrm{d}f'. \tag{26}$$

We replace the Raman contribution term with $-c_{\mathrm{R}}\beta(f,z)$, where $\beta(f,z)$ is given by

$$\beta(f,z)=\frac{\partial}{\partial f}\int_{f-\Delta_{\mathrm{R}}}^{f+\Delta_{\mathrm{R}}}(f-f')S(f',z)\mathrm{d}f'=P_{\Delta}(f,z)-\Delta_{\mathrm{R}}[S(f+\Delta_{\mathrm{R}},z) -S(f-\Delta_{\mathrm{R}},z)], \tag{27}$$

where $P_{\Delta}(f,z)$ is the total power within the triangular approximation window, given in (5).

The Raman contribution term is proportional to the power within the triangular window minus the power difference across the edges of the triangular window, multiplied by the triangular bandwidth. Assuming the tilt is small such that the power difference across the triangular bandwidth is negligible, and that the triangular bandwidth encompasses a sizeable portion of the total spectrum, we approximate the Raman contribution term as evolving proportionally to the total power:

$$\beta(f,z)\approx\beta(f,0)\frac{P_{\mathrm{T}}(z)}{P_{\mathrm{T}}(0)}. \tag{28}$$

Integrating (26) with respect to z, from 0 to z, we have

$$\frac{\partial}{\partial f}\ln\left[\frac{S(f,z)}{S(f,0)}\right]=-z\frac{\mathrm{d}\alpha(f)}{\mathrm{d}f}-c_{\mathrm{R}}\frac{\beta(f,0)}{P_{\mathrm{T}}(0)}\int_0^z P_{\mathrm{T}}(z')\mathrm{d}z', \tag{29}$$

and integrating with respect to f, from an arbitrary reference frequency f_{R}

$$\begin{aligned}\ln\left[\frac{S(f,z)S(f_{\mathrm{R}},0)}{S(f,0)S(f_{\mathrm{R}},z)}\right]&=\left[-\alpha(f')z-c_{\mathrm{R}}\Gamma(f')\int_0^z P_{\mathrm{T}}(z')\mathrm{d}z'\right]_{f'=f_{\mathrm{R}}}^{f}\\ S(f,z)&=\frac{S(f_{\mathrm{R}},z)}{S(f_{\mathrm{R}},0)}S(f,0)\exp\Big\{-\left[\alpha(f)-\alpha(f_{\mathrm{R}})\right]z\\ &\quad+c_{\mathrm{R}}\left[\Gamma(f_{\mathrm{R}})-\Gamma(f)\right]\int_0^z P_{\mathrm{T}}(0)\mathrm{d}z'\Big\},\end{aligned}\tag{30}$$

where $\Gamma(f)$ is the result of an improper integration of the powers involved within the Raman contribution term, normalized by the total launch power, and given by (4), where, arbitrary and with no impact to the final result, we set the lower integration boundary to the lower edge of the occupied spectrum.

We define f_{R} as the reference frequency with no ISRS-induced tilt, given as

$$S(f_{\mathrm{R}},z)=S(f_{\mathrm{R}},0)e^{-\alpha(f_{\mathrm{R}})z},\tag{31}$$

where we then obtain (3).

Appendix B
Derivation of the Total Power Attenuation Coefficient Expression

As the ISRS term in (3) should not incur in any instantaneous gain or losses to the total power, integrating (2) over the entire spectrum, we have that the total power evolution is dictated by

$$\frac{\mathrm{d}P_{\mathrm{T}}(z)}{\mathrm{d}z}=\int_{f_{\mathrm{Min}}}^{f_{\mathrm{Max}}}-\alpha(f')S(f',z)\mathrm{d}f',\tag{32}$$

where, under our approximation that $P_{\mathrm{T}}(z)=P_{\mathrm{T}}(0)e^{-\alpha_0 z}$, we have that the total power power evolution can also be rewritten as

$$\frac{\mathrm{d}P_{\mathrm{T}}(z)}{\mathrm{d}z}\approx-\alpha_0 P_{\mathrm{T}}(0)e^{-\alpha_0 z}.\tag{33}$$

From repeated derivations of (2) with respect to z, we also note that the ISRS does not instantaneously contributes to any higher order derivatives of the total power

$$\begin{aligned}\frac{\mathrm{d}^n P_{\mathrm{T}}(z)}{\mathrm{d}z^n}&=\int_{f_{\mathrm{Min}}}^{f_{\mathrm{Max}}}\frac{\partial^n S(f',z)}{\partial z^n}\mathrm{d}f'=\int_{f_{\mathrm{Min}}}^{f_{\mathrm{Max}}}[-\alpha(f)]^n S(f',z)\mathrm{d}f'\\ &\approx(-\alpha_0)^n P_{\mathrm{T}}(z),\end{aligned}\tag{34}$$

where we obtain infinitely many equations to solve for α_0, resulting in a free parameter n. Isolating α_0 from those solutions, and evaluation them at the fiber input ($z=0$), we obtain (9).

Appendix C
Derivation of the Shapping Function at the ISRS Tilt Reference Frequency

Expanding $S(f,z)$ in (34) with (3), considering the total power as exponentially decaying, and dividing both sides by $(-1)^n$ we have

$$\begin{aligned}\alpha_0^n P_{\mathrm{T}}(z)=&\int_{f_{\mathrm{Min}}}^{f_{\mathrm{Max}}}\alpha(f')^n S(f',0)\\ &\times e^{-\alpha(f')z+c_{\mathrm{R}}(\Gamma(f_{\mathrm{R}})-\Gamma(f'))P_{\mathrm{T}}(0)\frac{1-e^{-\alpha_0 z}}{\alpha_0}}\mathrm{d}f'.\end{aligned}\tag{35}$$

Isolating $\Gamma(f_{\mathrm{R}})$ from (35) we obtain a z-dependent expression for the shapping function at the zero-ISRS-tilt frequency. As the ISRS contribution of each channel evolves due to the evolving channel power spectral density, the reference zero-ISRS-tilt frequency also changes. However, assuming a constant value for f_{R} does not results in significant discrepancies to the power profile over the z domain, as seen in Fig. 4, with the benefit of reduced complexity to the closed-form model. Therefore, evaluating the solution of $\Gamma(f_{\mathrm{R}})$ at the fiber end ($z=L$), where it is of most interest, we obtain (10).

Appendix D
Derivation of the Total Power Attenuation and ISRS Tilt Reference Frequency With the Power Profiles at the Fiber Output

Considering an offset x from the fiber output, we can rewrite (34) as

$$\frac{\mathrm{d}P_{\mathrm{T}}(L-x)}{\mathrm{d}z}=\int_{f_{\mathrm{Min}}}^{f_{\mathrm{Max}}}\alpha(f')^n S(f',L-x)\mathrm{d}f'=\alpha_0^n P_{\mathrm{T}}(L)e^{\alpha_0 x}.\tag{36}$$

Isolating α_0 from (36), and evaluation it at the fiber output ($x\to 0$), we obtain (18).

The power spectral density term $S(f,L-x)$ at (35) can be expressed as a function of $S(f,L)$

$$S(f,L-z)=S(f,L)e^{\alpha(f)x-c_{\mathrm{R}}(\Gamma(f_{\mathrm{R}})-\Gamma(f))\int_{L-x}^{L}P_{\mathrm{T}}(x')\mathrm{d}x'},\tag{37}$$

where, under our assumption of an exponentially decaying total power, the total power integral can be given as a function of the received total power

$$\int_{L-x}^{L}P_{\mathrm{T}}(z')\mathrm{d}z'\approx P_{\mathrm{T}}(L)\frac{e^{\alpha_0 x}-1}{\alpha_0}.\tag{38}$$

Under similar steps to Appendix C, by expressing $S(f,L-x)$ as a function of $S(f,L)$, and evaluating f_{R} at the fiber end, from the general arbitrary order solution given in (36), we obtain

$$\begin{aligned}\Gamma(f_{\mathrm{R}})\approx\lim_{x\to 0}\frac{\alpha_0}{c_{\mathrm{R}}P_{\mathrm{T}}(L)(e^{\alpha_0 x}-1)}\ln\Bigg[&\int_{f_{\mathrm{Min}}}^{f_{\mathrm{Max}}}\frac{\alpha^n(f')S(f',L)}{\alpha_0^n P_{\mathrm{T}}(L)}\\ &\times e^{[\alpha(f')-\alpha_0]x+c_{\mathrm{R}}\Gamma(f')P_{\mathrm{T}}(L)\frac{e^{\alpha_0 x}-1}{\alpha_0}}\mathrm{d}f'\Bigg].\end{aligned}\tag{39}$$

where the limit appears as the integral of the solution is indetermined at $x=0$. Solving for the limit we obtain (19).

References

[1] P. J. Winzer and D. T. Neilson, "From scaling disparities to integrated parallelism: A decathlon for a decade," *Journal of Lightwave Technology*, vol. 35, no. 5, pp. 1099–1115, 2017.

[2] T. Hoshida, V. Curri, L. Galdino, D. T. Neilson, W. Forysiak, J. K. Fischer, T. Kato, and P. Poggiolini, "Ultrawideband systems and networks: Beyond C+ L-band," *Proceedings of the IEEE*, vol. 110, no. 11, pp. 1725–1741, 2022.

[3] K. Fukuchi, "Wideband and ultra-dense WDM transmission technologies toward over 10-Tb/s capacity," in *Optical Fiber Communication Conference*. Optica Publishing Group, 2002, p. ThX5.

[4] J. Renaudier, A. C. Meseguer, A. Ghazisaeidi, P. Tran, R. R. Muller, R. Brenot, A. Verdier, F. Blache, K. Mekhazni, B. Duval *et al.*, "First 100-nm continuous-band WDM transmission system with 115Tb/s transport over 100km using novel ultra-wideband semiconductor optical amplifiers," in *2017 European Conference on Optical Communication (ECOC)*. IEEE, 2017, pp. 1–3.

[5] J. Renaudier, A. Arnould, D. Le Gac, A. Ghazisaeidi, P. Brindel, M. Makhsiyan, A. Verdier, K. Mekhazni, F. Blache, H. Debregeas *et al.*, "107 Tb/s transmission of 103-nm bandwidth over 3× 100 km SSMF using ultra-wideband hybrid Raman/SOA repeaters," in *2019 Optical Fiber Communications Conference and Exhibition (OFC)*. IEEE, 2019, pp. 1–3.

[6] F. Hamaoka, K. Minoguchi, T. Sasai, A. Matsushita, M. Nakamura, S. Okamoto, E. Yamazaki, and Y. Kisaka, "150.3-tb/s ultra-wideband (s, c, and l bands) single-mode fibre transmission over 40-km using¿ 519gb/s/a pdm-128qam signals," in *2018 European Conference on Optical Communication (ECOC)*. IEEE, 2018, pp. 1–3.

[7] L. Galdino, A. Edwards, W. Yi, E. Sillekens, Y. Wakayama, T. Gerard, W. S. Pelouch, S. Barnes, T. Tsuritani, R. I. Killey *et al.*, "Optical fibre capacity optimisation via continuous bandwidth amplification and geometric shaping," *IEEE Photonics Technology Letters*, vol. 32, no. 17, pp. 1021–1024, 2020.

[8] B. J. Puttnam, R. S. Luís, G. Rademacher, M. Mendez-Astudillio, Y. Awaji, and H. Furukawa, "S-, C-and L-band transmission over a 157 nm bandwidth using doped fiber and distributed Raman amplification," *Optics Express*, vol. 30, no. 6, pp. 10 011–10 018, 2022.

[9] A. Chraplyvy, "Optical power limits in multi-channel wavelength-division-multiplexed systems due to stimulated Raman scattering," *Electronics letters*, vol. 20, no. 2, pp. 58–59, 1984.

[10] A. R. Chraplyvy, "Limitations on lightwave communications imposed by optical-fiber nonlinearities," *Journal of Lightwave Technology*, vol. 8, no. 10, pp. 1548–1557, 1990.

[11] R. Stolen and E. Ippen, "Raman gain in glass optical waveguides," *Applied Physics Letters*, vol. 22, no. 6, pp. 276–278, 1973.

[12] D. Semrau, R. Killey, and P. Bayvel, "Achievable rate degradation of ultra-wideband coherent fiber communication systems due to stimulated Raman scattering," *Optics express*, vol. 25, no. 12, pp. 13 024–13 034, 2017.

[13] M. Cantono, D. Pilori, A. Ferrari, C. Catanese, J. Thouras, J.-L. Augé, and V. Curri, "On the interplay of nonlinear interference generation with stimulated Raman scattering for QoT estimation," *Journal of Lightwave Technology*, vol. 36, no. 15, pp. 3131–3141, 2018.

[14] D. Semrau, E. Sillekens, P. Bayvel, and R. I. Killey, "Modeling and mitigation of fiber nonlinearity in wideband optical signal transmission," *Journal of Optical Communications and Networking*, vol. 12, no. 6, pp. C68–C76, 2020.

[15] S. Okamoto, K. Minoguchi, F. Hamaoka, K. Horikoshi, A. Matsushita, M. Nakamura, E. Yamazaki, and Y. Kisaka, "A study on the effect of ultra-wide band WDM on optical transmission systems," *Journal of Lightwave Technology*, vol. 38, no. 5, pp. 1061–1070, 2020.

[16] C. Lasagni, P. Serena, A. Bononi, and J.-C. Antona, "A generalized Raman scattering model for real-time SNR estimation of multi-band systems," *Journal of Lightwave Technology*, vol. 41, no. 11, pp. 3407–3416, 2023.

[17] I. Roberts, J. M. Kahn, J. Harley, and D. W. Boertjes, "Channel power optimization of WDM systems following Gaussian noise nonlinearity model in presence of stimulated Raman scattering," *Journal of Lightwave Technology*, vol. 35, no. 23, pp. 5237–5249, 2017.

[18] M. Jarmolovičius, D. Semrau, H. Buglia, M. Shevchenko, F. M. Ferreira, E. Sillekens, P. Bayvel, and R. I. Killey, "Optimising O-to-U band transmission using fast ISRS Gaussian noise numerical integral model," *Journal of Lightwave Technology*, 2024.

[19] Y. Jiang, J. Sarkis, A. Nespola, F. Forghieri, S. Piciaccia, A. Tanzi, M. R. Zefreh, and P. Poggiolini, "Optimization of long-haul C+ L+ S systems by means of a closed form EGN model," *IEEE Photonics Technology Letters*, 2024.

[20] H. Buglia, E. Sillekens, A. Vasylchenkova, P. Bayvel, and L. Galdino, "On the impact of launch power optimization and transceiver noise on the performance of ultra-wideband transmission systems," *Journal of Optical Communications and Networking*, vol. 14, no. 5, pp. B11–B21, 2022.

[21] A. Vasylchenkova, H. Buglia, E. Sillekens, R. I. Killey, and P. Bayvel, "Launch power optimisation for ultrawideband transmission: Achievable throughput improvement under practical constraints," in *IET Conference Proceedings CP839*, vol. 2023, no. 34. IET, 2023, pp. 1051–1054.

[22] H. Buglia, E. Sillekens, L. Galdino, R. Killey, and P. Bayvel, "Throughput maximisation in ultra-wideband hybrid-amplified links," in *Optical Fiber Communication Conference*. Optica Publishing Group, 2024, pp. Tu3H–5.

[23] J. Yang, H. Buglia, M. Jarmolovičius, R. Aparecido, E. Sillekens, R. Sohanpal, M. Tan, D. Pratiwi, R. S. Luis, B. J. Puttnam *et al.*, "122.6 Tb/s S+ C+ L Band Unrepeatered Transmission Over 223 km Link With Optimized Bidirectional Raman Amplification," *Journal of Lightwave Technology*, vol. 43, no. 4, pp. 1893–1901, 2025.

[24] Y. Jiang, J. Sarkis, S. Piciaccia, F. Forghieri, and P. Poggiolini, "Signal and Backward Raman Pump Power Optimization in Multi-Band Systems Using Reliable and Fast Power Profile Estimation," *Journal of Lightwave Technology*, 2025.

[25] D. Christodoulides and R. Jander, "Evolution of stimulated Raman crosstalk in wavelength division multiplexed systems," *IEEE Photonics Technology Letters*, vol. 8, no. 12, pp. 1722–1724, 1996.

[26] M. Zirngibl, "Analytical model of Raman gain effects in massive wavelength division multiplexed transmission systems," *Electronics letters*, vol. 34, no. 8, pp. 789–790, 1998.

[27] P. Poggiolini, "A generalized GN-model closed-form formula," *arXiv preprint arXiv:1810.06545*, 2018.

[28] M. R. Zefreh and P. Poggiolini, "A real-time closed-form model for non-linearity modeling in ultra-wide-band optical fiber links accounting for inter-channel stimulated Raman scattering and co-propagating Raman amplification," *arXiv preprint arXiv:2006.03088*, 2020.

[29] N. A. Shevchenko, S. Nallaperuma, and S. J. Savory, "Maximizing the information throughput of ultra-wideband fiber-optic communication systems," *Optics express*, vol. 30, no. 11, pp. 19 320–19 331, 2022.

[30] S. Tariq and J. C. Palais, "A computer model of non-dispersion-limited stimulated Raman scattering in optical fiber multiple-channel communications," *Journal of lightwave technology*, vol. 11, no. 12, pp. 1914–1924, 2002.

[31] J. Bromage, "Raman amplification for fiber communications systems," *journal of lightwave technology*, vol. 22, no. 1, p. 79, 2004.

[32] K. Rottwitt, J. Bromage, A. J. Stentz, L. Leng, M. E. Lines, and H. Smith, "Scaling of the Raman gain coefficient: applications to germanosilicate fibers," *Journal of lightwave technology*, vol. 21, no. 7, pp. 1652–1662, 2003.

[33] K. J. Cordina and C. R. Fludger, "Changes in Raman gain coefficient with pump wavelength in modern transmission fibres," in *Optical Amplifiers and their Applications*. Optica Publishing Group, 2002, p. OMC3.

[34] H. Buglia, M. Jarmolovičius, L. Galdino, R. I. Killey, and P. Bayvel, "A closed-form expression for the Gaussian noise model in the presence of Raman amplification," *Journal of Lightwave Technology*, vol. 42, no. 2, pp. 636–648, 2023.

[35] R. H. Stolen, J. P. Gordon, W. Tomlinson, and H. A. Haus, "Raman response function of silica-core fibers," *JOSA B*, vol. 6, no. 6, pp. 1159–1166, 1989.

[36] Q. Lin and G. P. Agrawal, "Raman response function for silica fibers," *Optics letters*, vol. 31, no. 21, pp. 3086–3088, 2006.

[37] S. Walker, "Rapid modeling and estimation of total spectral loss in optical fibers," *Journal of lightwave technology*, vol. 4, no. 8, pp. 1125–1131, 1986.

[38] M. Cantono, R. Schmogrow, M. Newland, V. Vusirikala, and T. Hofmeister, "Opportunities and challenges of C+ L transmission systems," *Journal of Lightwave Technology*, vol. 38, no. 5, pp. 1050–1060, 2020.

[39] C. Lasagni, P. Serena, and A. Bononi, "Modeling nonlinear interference with sparse Raman-tilt equalization," *Journal of Lightwave Technology*, vol. 39, no. 15, pp. 4980–4989, 2021.

[40] A. Ferrari, A. Napoli, J. K. Fischer, N. Costa, A. D'Amico, J. Pedro, W. Forysiak, E. Pincemin, A. Lord, A. Stavdas *et al.*, "Assessment on the achievable throughput of multi-band ITU-T G. 652. D fiber transmission systems," *Journal of Lightwave Technology*, vol. 38, no. 16, pp. 4279–4291, 2020.

[41] N. Taengnoi, K. R. Bottrill, Y. Hong, L. Hanzo, and P. Petropoulos, "Ultra-long-span U-band transmission enabled by incoherently pumped Raman amplification," *Journal of Lightwave Technology*, vol. 41, no. 12, pp. 3767–3773, 2023.